Journal of Applied Pharmaceutical Research
Volume 12 Issue 3, Year of Publication 2024, Page 138 – 157
DOI: https://doi.org/10.69857/joapr.v12i3.581

Check for updates

Research Article

JOURNAL OF APPLIED PHARMACEUTICAL RESEARCH | JOAPR
www.japtronline.com ***ISSN: 2348 – 0335***

OPTIMIZING IRBESARTAN SPHERICAL AGGLOMERATES THROUGH PRINCIPAL COMPONENT ANALYSIS AND EXPERIMENTAL DESIGN

V. D. Gorde[1]*, Punit R. Rachh[1], Someshwar Mankar[2], Saurin Amin[3]

Article Information
Received: 14th February 2024
Revised: 28th April 2024
Accepted: 22nd May 2024
Published: 30th June 2024

Keywords
Central composite design, Packing and compaction, Flow property, Kawakita analysis, Principal component analysis

ABSTRACT
Background: This study explores the amalgamation of crystallization and agglomeration through spherical crystallization, aiming to develop the spherical crystals of Irbesartan with improved micromeritic properties. The main objective is to use spherical crystallization techniques to improve the micromeritic characteristics of Irbesartan, which has poor flow and compressibility because of its crystal habit. **Methodology**: A solvent change approach was utilized to synthesize spherical agglomerates of Irbesartan. Several system parameters, including the amount of bridging liquid, the rate of stirring, and the concentration of the polymer, were tuned to enhance the particle size distribution and mechanical qualities. SEM, GC, PXRD, DSC, and FTIR analyses characterised the spherical crystals. **Result and Discussion**: The study demonstrated that spherical crystallization significantly enhanced Irbesartan's micromeritic properties. The angle of repose of optimized agglomerates was reduced by around 52%, indicating improved considerably flowability of irbesartan. The sphericity of the crystals was validated by SEM examination (shape factor: 0.996), and the solvent levels were found to be within allowable bounds by GC analysis. PXRD data showed no polymorphism alterations, and DSC/FTIR analyses confirmed that the excipients and drug were compatible. **Conclusion**: This process provides a feasible alternative to classic granulation and agglomeration procedures, resulting in better flow, compressibility, and spherical crystals. It streamlines the Irbesartan formulation, improving efficiency and uniformity, reducing manufacturing costs, higher tablet consistency, and enhancing patient compliance.

INTRODUCTION

The development and application of spherical crystallization in pharmaceutical sciences have significantly advanced since its initial discovery by Kawashima et al. in the 1980s [1,2]. This unique particle engineering methodology was developed to overcome the limits of previous granulation and agglomeration techniques, frequently producing particles with poor flow and compressibility qualities. Spherical crystallization converts crystalline particles into spherical agglomerates, improving their flowability, compressibility, and packing properties – all of which are crucial in efficient pharmaceutical manufacture. Spherical crystallization was initially used to improve the

[1]*Department of Pharmaceutical Science, Bhagwant University, Ajmer, Rajasthan, India*
[2]*Pravara Rural College of Pharmacy, Loni, Maharastra, India*
[3]*Gujarat Technological University, Gujarat, India*

For Correspondence:** **vikasgorde007@gmail.com

handling and processing of bulk drug powders. Still, it has gained widespread acceptance and application to various pharmaceutical compounds, particularly in increasing the solubility, dissolution rate, and bioavailability of poorly water-soluble drugs [2]. Recent advances in techniques such as quasi-emulsion solvent diffusion and spherical agglomeration have enhanced the process, broadening its possibilities and benefits while establishing the method as a cornerstone of modern pharmaceutical manufacture. Such advancements promise to revolutionize drug delivery systems, offering improved efficacy and stability in pharmaceutical products. The development and application of spherical crystallization in pharmaceutical sciences have advanced significantly since its initial discovery by Kawashima *et al.* in the 1980s. This innovative particle engineering method was created to overcome the limitations of earlier granulation and agglomeration techniques, which often produced particles with poor flow and compressibility properties. Spherical crystallization transforms crystalline particles into spherical agglomerates, enhancing their flowability, compressibility, and packing properties—crucial factors in efficient pharmaceutical manufacturing. Initially, spherical crystallization was employed to improve the handling and processing of bulk drug powders. Over time, it has gained widespread acceptance for various pharmaceutical compounds, particularly in improving poorly water-soluble drugs' solubility, dissolution rate, and bioavailability. Recent advances in methods such as quasi-emulsion solvent diffusion and spherical agglomeration have expanded the process's potential and benefits, solidifying its role in modern pharmaceutical manufacturing. The flexible method allows the ability to regulate the size and kind of crystals. Through particle engineering, crystals can be directly transformed into compressed spherical form by agglomerating and crystallizing concurrently in a single step. Because crystal habit (form, surface, size, and particle size distribution) can be altered throughout the crystallization process, the particle above design approach has become one of the active research areas currently of interest in pharmaceutical manufacturing. It has also recently obtained excellent popularity and significance. Certain physicochemical qualities like solubility, dissolution rate, bioavailability, stability, and micromeritic characteristics like bulk density, flow property, and compatibility may also shift due to such variations in the crystal habit [3]. New particulate drug delivery systems such as microsponges, microspheres and nanospheres, micro balloons, nanoparticles, and micro pellets can also be created. With this approach, certain medications with a sluggish dissolution profile and limited water solubility may change from their crystalline form to a new polymorphic form, increasing their bioavailability and dissolving more quickly. Through this innovative approach, the physicochemical attributes of pharmaceutical crystals undergo remarkable enhancement, optimizing pharmaceutical processes like milling, mixing, and tableting due to their outstanding flow and compaction characteristics. This method is straightforward and cost-effective for large-scale production and streamlines operations, requiring fewer resources and personnel, thus minimizing time and expenses [4]. This advancement marks a significant milestone in tableting technology, particularly integrating various directly compressible excipients. Furthermore, the spherical agglomerated crystals can be readily formulated into tablets or directly incorporated into pharmaceutical systems without additional processing steps like granulation. Principal component analysis (PCA) is utilized when you have collected data on numerous observed variables and aim to condense them into a smaller set of artificial variables, known as principal components, which capture the majority of the variability present in the original variables. This method proves beneficial when there is redundancy among the variables, indicating that some variables may be correlated due to measuring similar constructs. By reducing the observed variables into principal components, PCA aids in simplifying the dataset while retaining essential information [5]. Although PCA shares similarities with exploratory factor analysis (EFA) regarding procedural steps, it is crucial to recognize the conceptual distinctions between the two techniques to avoid misinterpretation or misapplication. The pharmaceutical sector favors the direct compression method over all others regarding tablet formulation. Good compression and flow qualities of the powder or blend are essential for this process [6]. Direct compression, however, is highly dependent on the powder's flow properties, which can be enhanced by adding various glidants or flow enhancers. Optimizing compression properties is still difficult to achieve, even with changes to processing processes or excipients [7]. Many crystalline medications and excipients are fluffy and have low relative bulk and tapped densities, exacerbating direct compression problems [8]. Irbesartan, renowned for its antihypertensive properties, is an AT1 receptor antagonist [9]. Characterized by its crystalline nature with an acicular morphology, it presents a fluffy texture alongside comparatively low tapped and bulk densities [10]. Despite its

efficacy, these inherent traits lead to suboptimal flow and compression behaviors, complicating the formulation of directly compressible tablets. Consequently, leveraging spherical agglomeration is a promising strategy to ameliorate its flow and compaction characteristics, facilitating tablet formulation processes. Bridging Liquid Amount: Essential for particle wetting and binding, ensuring proper agglomeration and uniform shape. Stirring Rate: Influences size and uniformity of agglomerates; controlled stirring prevents excessive aggregation. Polymer Concentration: Affects surface characteristics and stabilizes agglomerates, enhancing mechanical strength and compressibility. There are various major critical issues in pharmaceutical product development, particularly those related to bulk drug powders' poor flowability, compressibility, and solubility. Traditional granulation and agglomeration processes frequently fail to create particles with the correct physical qualities, resulting in industrial inefficiencies and poor medication compositions. This study's methodological rationale stems from advanced spherical crystallization procedures, which convert crystalline particles into spherical agglomerates, greatly enhancing flow and compressibility. This work is crucial because it improves Irbesartan's manufacturing efficiency (very poorly flowable) as an antihypertensive agent and maintains better product quality and patient compliance.

MATERIALS AND METHODS

Materials

Irbesartan was obtained from CTX Lifescience Pvt. Ltd., India, while talc, PEG 6000, and PVA were acquired from HiMedia Labs in Mumbai, India. HPMC was generously provided by Colorcon Asia Pvt. Ltd. in Goa, India, and Eudragit was received as a gift from Evonik in Mumbai. High-performance liquid chromatography (HPLC) grade acetonitrile and water were sourced from Merck Pvt. Ltd. in Mumbai, India. All other chemicals utilized were of analytical grade and obtained from Merck Pvt. Ltd. in Mumbai, India. Double-distilled water was used throughout the study.

METHODOLOGY

Formulation of spherical agglomerates

Solvent system selection

To determine the solubility of Irbesartan, we employed the shake flask method [11]. An excess of Irbesartan was introduced into 5mL volumetric flasks, each containing 2mL of varying solvents. These flasks were then placed on a rotary shaker for 24 hours. Following equilibrium, the samples were extracted from the shaker and centrifuged at 2500 RPM for 10 minutes. After appropriate dilution with methanol, the resulting supernatant was analyzed for drug content using a UV spectrophotometer.

Selection of excipients and processing parameters

Various additives were added to suitable solvents at different levels to determine their effect on the development of agglomerates of irbesartan. These excipients included talc, polyvinyl pyrrolidone K30 (PVP), hydroxypropyl cellulose (HPC), ethyl cellulose (EC), hydroxypropyl methylcellulose K4M (HPMC), polyvinyl alcohol (PVA), polyethylene glycol 6000 (PEG), and eudragit E 100 (ERE). While keeping other variables like stirring speed, temperature, and phase ratio constant, initial experiments were carried out to optimize the types and concentrations of polymers. Crushing strength (CS), angle of repose (AoR), and mean geometric dimension (dg) served as the selection criteria. Employing a propeller-type agitator at room temperature, an optimized batch of agglomerates containing particular additives was evaluated at various stirring rates (100–1200 rpm) to analyze dg, AoR, and CS. The temperature impact was then investigated by preparing the optimized batch at different temperatures and measuring dg, AoR, and CS. In addition, various proportions of good to poor solvents have been utilized to assess the impact of phase ratio on spherical crystallization. The amount of bridging liquid, stirring rate and polymer concentration are all important criteria when optimizing the spherical crystallization process because they directly impact the final product qualities. The amount of bridging liquid affects agglomeration and shape uniformity, ensuring particle wetting and binding. The stirring rate influences the size and regularity of the agglomerates, with controlled churning facilitating constant particle growth while preventing aggregation. Polymer concentration alters surface characteristics and stabilizes agglomerates, increasing mechanical strength and compressibility. Together, these factors ensure the formation of spherical agglomerates with outstanding flow properties, compressibility, and homogeneity, which are critical for the efficient fabrication and performance of Irbesartan formulations.

Technique used to prepare spherical agglomerates

The IRB was dissolved in a suitable solvent together with preset polymer concentrations. Following dissolving, bridging liquid

was gradually added while the mixture was constantly stirred using a mechanical stirrer to promote agglomeration. The stirring parameters were carefully monitored to guarantee homogeneous particle development and aggregation. Temperature was kept constant throughout the process to enhance crystallization kinetics. The resultant agglomerates were filtered through filter paper and washed with distilled water to eliminate leftover solvents and contaminants [12]. Following filtration, the agglomerates were dried at room temperature for 24 hours and kept in a desiccator to avoid moisture absorption. Various polymers (HPMC, PVP, PVA, PEG, and Eudragit) were used singly and in combinations to customize the agglomeration properties, assuring optimal flow, compressibility, and stability for pharmaceutical applications. Each evaluation was performed three times, and mean±standard deviation (SD) values were reported to demonstrate reproducibility.

Central composite design

The Central Composite Design (CCD) was chosen for this investigation because of its reliability and efficiency in optimizing processes with various variables. Unlike the Box-Behnken design, CCD incorporates both factorial and axial points, allowing for a more thorough examination of the response surface. This enables a more accurate estimation of curvature and interaction effects, which is crucial for understanding the complicated interactions between the variables that influence Irbesartan spherical agglomeration. CCD's ability to effectively fit a quadratic model with a small number of experimental runs makes it ideal for our study's goal of improving several formulation parameters while maintaining high precision and dependability in the results. The amount of talc and agitation speed play a crucial role in preparing IRB agglomerates. Central composite design (CCD) [13] was employed for the systemic study of joint influence of the effect of independent variables [Amount of Talc (X_1) and agitation speed (X_2)] on responses such as particle size (PS), crushing strength (CS), angle of repose (AoR) and yield (YLD). Based on preliminary trials, two factors and their levels were decided: the amount of talc (X_1): 2.5-4.5 %w/w and speed of agitation (X_2): 600-900 rpm. In this design, two factors with five levels (Table 1) were probed to investigate the main effects and interaction of the two factors on fourteen responses. Dependent variables were selected based on results obtained after applying principal component analysis (PCA). The design consists of nine runs (4 factorial points, 4-star points, and 5 center points), yielding 13 experiments in total (Table 1). A quadratic model incorporating interactive and polynomial terms was used to evaluate the response. $Y_i = b_0 + b_1X_1 + b_2X_2 + b_{11}X_1^2 + b_{22}X_2^2 + b_{12}X_1X_2$ where Yi was the dependent variable, b0 was the arithmetic mean response of the 9 runs, and b_i was the estimated coefficient for factor X_i. The main effects (X_1 and X_2) represent the average result of changing one factor from its low to high value at a time. The interaction term(X_1X_2) shows how the response changes when two factors are simultaneously changed. The polynomial terms (X_1^2 and X_2^2) were included to investigate nonlinearity. Data were further analyzed using Microsoft Excel® 2013 for regression analysis. One-way analysis of variance (ANOVA) was implemented to ensure no significant difference between the developed full model and the reduced model. The significance level was commonly selected at $p<0.05$, suggesting a 95% confidence level in deciding whether observed variations among the means of distinct groups were statistically significant or occurred by chance. Response surface plots were plotted to study response variations against two independent variables using Design Expert 13 (Stat-Ease. Inc. Minneapolis, USA) software.

Table 1: CCD layout congaing factors and levels

Batch	Independent variables				
	X_1	X_2			
C1	-1	-1			
C2	+1	-1			
C3	-1	+1			
C4	+1	+1			
C5	-α*	0			
C6	+α	0			
C7	0	-α			
C8	0	+α			
C9 – C13	0	0			
Factor	Level				
	-α	**-1**	**0**	**1**	**α**
X_1: Amount of talc (% w/w)	2.08	2.5	3.5	4.5	4.91
X_2: Agitation speed (rpm)	538	600	750	900	962

*α 1.414

Design Expert software was utilized to select the point batch (optimized batch). The model was further validated by evaluating % relative error between the predicted and experimental response for the point batch using the following formula:

$$\%RE = \frac{Predicted\ Value - Experimental\ Value}{Predicted\ Value} \times 100 \qquad \text{(Eq. 1)}$$

Characterization of agglomerates

Drug content and percent yield

Properly measured and crushed IRB agglomerates equal to 100 mg of Irbesartan were then put into a standard conical flask with a capacity of 100 mL. To dissolve the medication and the polymer, methanol was added, and the mixture was sonicated for five to ten minutes in a sonicator. Methanol was added to the quantity to reach 100 mL, and then Whatman paper was used to purify the mixture. After the filter was obtained, 0.5 mL of the solution was removed and adjusted to create 10 µg/ml. A UV visible spectrum analyzer determined the absorbance at 245.95 nm compared to a blank reagent. The calibration curve was used to calculate the drug's concentration in the formulation. Every sample underwent triplicate analysis. The following formula determined the samples' percent (%) yield [14]. The mean value was determined for both parameters by averaging the three determinations.

$$\%\, Yield = \frac{Total\ weight\ of\ agglomerates}{Total\ weight\ of\ drug\ and\ excipients} \times 100 \qquad \text{(Eq. 2)}$$

Particle size and shape

The optical microscopy method was used to determine the size and form of the particles. The ocular disc, earlier calibrated using a stage micrometer, was the basic optical microscope eye component [15]. The particle size distribution curve was created, the size was determined, and the mean geometric diameter (dg) was computed. The spherical agglomerates are examined using an optical microscope to study their shape. Agglomerate photomicrographs were examined for sphericity and surface morphology. Area (A) and perimeter (P') were used to calculate the shape factor (SF), irregularity factor (IF), and circularity factor (CF) for agglomerates. The total surface and circumference of the agglomerates were measured using the tracings of their enlarged photomicrographs [5,16]. By dividing the maximum diameter by the diameter at a right angle to it, the aspect ratio (AR) was determined.

$$Shape\ factor(SF) = P"/P' \qquad \text{(Eq. 3)}$$

$$Circularity\ factor(CF) = \frac{P'^2}{4\pi A} \qquad \text{(Eq. 4)}$$

$$Irregularity\ factor\ (IR) = \frac{Area}{Perimeter\ (P')} \qquad \text{(Eq. 5)}$$

$$Aspect\ ratio(AR) = \frac{Dmax}{Dmin} \qquad \text{(Eq. 6)}$$

where, P" =2π $(A/\pi)^{1/2}$, D_{max} = maximum diameter of the agglomerate, D_{min}= diameter measured to right angle to D_{max}.

Flow characteristics

The angle of repose is a prevalent technique for evaluating flow properties, typically assessed through the fixed funnel method [17]. Additionally, the flowability of both untreated and agglomerated samples was evaluated using Carr's Index (CI) and Hausner's ratio (HR) [18]. The final results were determined based on the average of three measurements.

Compression behavior analysis

Particles must have advantageous compression and compaction properties to participate in the direct compression process. To evaluate the powder's and optimized agglomerates' compaction behavior, plots connecting relative volume to compression were created.

Heckel analysis

IRB powder and agglomerates (500±5 mg) were compressed for one minute using a KBr press and an 8 mm flat-faced punch at different compaction. A 1%w/v magnesium stearate in acetone dispersion was used to lubricate the punch and die. The agglomerates were compressed at a weight of seven tonnes to create compacts with no porosity [19]. The Heckel formula,

$$ln\frac{1}{1-D} = KP + A \qquad \text{(Eq. 7)}$$

was utilized. In this formula, P stands for compaction pressure (tonnes), D for packing fraction, and K and A are constants. The inverse of K is the mean yield pressure.

Kawakita Study

A precise amount of the powder and agglomerate samples were meticulously put into a 10 mL measuring cylinder for the Kawakita investigation [20]. Then, to determine the volume drop after every two taps, this cylinder was placed into the tapped density apparatus. Through the application of the formula

$$\frac{n}{C} = \frac{1}{ab} + \frac{n}{a} \qquad \text{(Eq. 8)}$$

where, constants 'a' and 'b' were ascertained by graphing n/C against the number of taps. In this instance, 'C' is the volume reduction coefficient computed as (Vo – Vn)/Vo, where 'n' is the number of taps and 'Vo' and 'Vn' are the first and second tapped volumes, respectively.

Kuno analysis

The findings from the Kawakita study served as the basis for the subsequent Kuno analysis [21]. The Kuno analysis employed the equation:

$$\rho f - \rho n = (\rho f - \rho o) \cdot e^{-kn} \qquad \text{(Eq. 9)}$$

where ρf, ρn, and ρo represent the density of the powder bed at the final, nth, and initial stages, respectively. 'n' denotes the

number of tapings, and 'k' signifies the Kuno constant. A logarithmic plot of (ρf- ρn) against the number of tapings (n) facilitated the determination of the Kuno constant, indicating the rate of packability.

Elastic recovery

To assess the elastic recovery, compacts utilized in the Heckel plot analysis were allowed to rest for a full day following the measurement of their diameter and thickness [22]. The compact thickness was determined both immediately after ejection (Hc) and 24 hours later during the relaxation phase (He). The equation below was used to compute elastic recovery.

$$\%ER = \frac{He-Hc}{Hc} \times 100 \qquad \text{(Eq. 10)}$$

Crushing strength

Crushing strength (CS) is a direct indicator of compact mechanical durability, so it is used to calculate mechanical strength. The mercury load cell technique was used to figure it out. Employing a 10-milliliter hypodermic glass syringe, the mercury-loaded cell technique was used to assess the crushing strength of the developed agglomerates [23,24]. The syringe was positioned beneath the agglomeration, and mercury was injected via the empty injection tube. The aggregate's crushing strength was determined by the total weight of the mercury-filled tube at the point of breakage.

Tensile strength

500 mg were compressed for one minute using a KBr press at different pressure settings (measured in tons/cm²) to evaluate the tensile strength of spherical agglomerates. After recording the compact's thickness and diameter, it was kept in a desiccator for the entire night to aid in plastic recovery. A Pfizer hardness tester was then used to determine the compact's hardness. Using the following formula, the compact's tensile strength (σ), which is measured in tons/cm², was determined [25].

$$\sigma = \frac{2F}{\pi Dt} \qquad \text{(Eq. 11)}$$

where F= Hardness of compact, D= Diameter, t= thickness

Fourier transform infrared (FTIR) spectroscopy

Using an FTIR spectrophotometer, the FTIR spectra of optimized agglomerates and untreated IRB were captured in the 4000–400 cm^{-1} wavelength range [26]. An appropriate amount of samples (about 1% w/w) were combined with KBr powder and added to a sample container.

Differential Scanning Calorimetry (DSC)

Thermograms of IRB and agglomerates were collected using a differential scanning calorimeter (DSC). Agglomerates of the optimized batch and an accurately weighted sample of IRB were hermetically sealed in an aluminum crucible [11]. To keep the atmosphere inert, the system was purged with ultra-high quality nitrogen gas at a 20 mL/min flow rate. At 10°C per minute, heating was done from 10 to 300°C.

X-Ray Powder Diffraction (XPRD)

Using Cu Kα-1 radiation (λ = 1.542 Å) at 30 kV voltage and 30 mA current, powder X-ray diffraction patterns of the pure IRB and agglomerates of the optimized batch were produced (X-ray diffractometer, Brucker D8 Advanced). Using a chart speed of 5 mm/2°, the data was captured at a scanning rate of 1×104C/sec over a range of 5° to 80° [27].

Scanning Electron Microscopy (SEM)

Scanning electron microscopy was used to determine the surface topography and measure the particle size [28]. The agglomerates were packed on the aluminum stub using double sticky tape. The Zeiss Evo 15 scanning electron microscope was used to capture the scanning electron micrographs of both pure drugs and agglomerates.

Gas chromatography (GC)

Following the dissolution of 300±2 mg of IRB and an optimized batch of agglomerates in methanol, the filtrate was filtered and subjected to GC-MS QP 2010 (Shimadzu, Japan) analysis utilizing column Rtx-5MS (thickness: 0.25 m, diameter: 0.25 m, length: 60 m) and helium as the carrier gas [29]. The area of the peak obtained after injecting the reference solution (DMF and Toluene) and sample solutions alternatively into GC-HS was used to determine the concentration of DMF and Toluene in agglomerates.

In Vitro Dissolution

Using a type II (Electrolab, TDT 06P) dissolution apparatus (Basket type), an *in vitro* dissolution study was conducted on pure drug and manufactured spherical agglomerates to assess the impact of the polymer used on drug release from the agglomerates in 900mL of 0.1N HCl at 37±0.5°C and 50 RPM. 5 mL aliquots were removed at prearranged intervals and replaced with an equivalent volume of dissolving fluid. After an appropriate dilution, the samples were examined

spectrophotometrically at 246.09nm. Then, the absorbance was measured at 247.35nm, and a graph showing the cumulative percentage of drug release v/s time was shown. 2 hour buffer medium was then changed to phosphate buffer pH 6.8 [30].

Stability study

For three months, the agglomerates were charged in a stability chamber at 40±2°C and 75±5% relative humidity by ICH recommendations for accelerated stability tests. USP type-1 flint vials containing this formulation were filled and covered with aluminum caps. After being removed from the samples every 30 days, the drug content, mean geometric diameter, crushing strength, and in vitro drug release were assessed [31].

Principal component analysis

The Unscrambler®10.2 program (CAMO AS, Norway) was used to group the materials and apply PCA to uncover hidden structures in the data set. The previously mentioned materials (objects, = 13) with different parameters (variables, p = 14) for each were put in the data matrix. Systematic cross-validation was used for PCA modeling, and a popular normalization technique (1/SDev) was used to scale and center the data [32]. A methodical approach was used, including pure IRB and agglomerates in the model and ending with identifying extremes or possible outliers [5]. Then, extreme samples were excluded to conduct a more thorough analysis of the remaining materials.

RESULT AND DISCUSSION

Formulation of spherical agglomerates

Selection of solvent system

A drug's solubility in various solvents must be investigated before doing crystallization tests. The drug's solubility characteristics aid in selecting appropriate solvents. Higher solubility solvents are selected as excellent solvents, whereas lower solubility solvents are labeled bad solvents [33]. Furthermore, a bridging solvent is chosen to have restricted solubility and be immiscible with both the anti-solvent and the medication. For instance, several pure solvents, including hexane, water, chloroform, carbon tetrachloride, DCM, n-butanol, toluene, ethanol, ethyl acetate, methanol, acetone, DMF, and petroleum ether, were used in a solubility investigation of IRB. Figure 1 presents a graphic representation of the study's findings. The results of the solubility investigation revealed that IRB exhibits the highest solubility in DMF compared to other solvents, making it a favorable choice. Petroleum ether, on the other hand, showed the least solubility, suggesting that it is not a good solvent. Petroleum ether was not included because of safety concerns related to its use, even though it was effective [34]. When evaluated as a substitute weak solvent, water produced encouraging results regarding the recrystallization of IRB. Furthermore, IRB's low water solubility—confirmed by the solubility investigation, which produced a solubility of 0.907 mg/mL in water—leads to its classification as a BCS-II medication. The immiscibility of the bridging liquid with the weak solvent (water) led to its selection, as it is crucial for wetting the drug during IRB recrystallization.

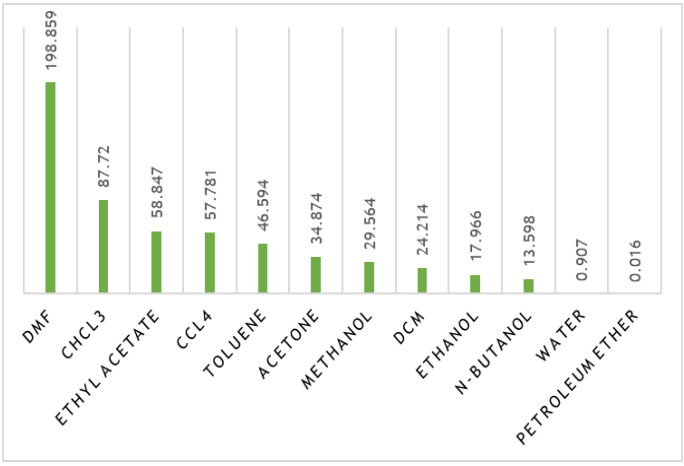

Figure 1: Solubility (mg/mL) of IRB in different solvents

Preparation of Spherical agglomerates

For the formulation process, a range of polymers (PEG 6000, Eudragit E100, HPC, HPMC K4M, PVP K30, PVA, and Talc) and their mixes were used. Each batch's crushing strength (CS) and angle of repose (AoR) were evaluated. Following a thorough analysis, the polymer combination with the highest CS and lowest AoR was selected. Early analyses of the process parameters showed that the micromeritics properties of spherical agglomerates were significantly influenced by variables including talc content (%w/w) (X1) and agitation speed (RPM) (X2). These factors were, therefore, selected for additional systematic investigation. Four dependent variables were evaluated for each of the thirteen batches of agglomerates and IRB, including shape factor, circularity factor, aspect ratio, irregularity factor, drug content, yield, particle size, and crushing strength. These variables included Hausner's ratio, Carr's index, and Kawakita and Kuno analyses. This analysis revealed that X1 and X2 had a major impact on these answers (Table 2).

Table 2: a) **Evaluation of experimental design batches***

Batch	a[a]	b[aa]	k[b]	AoR[c](°)	PS[d](µm)	CI[e] (%)	HR[f]
IRB	0.191 ± 0.015	0.156 ± 0.001	0.071 ± 0.005	44.23 ± 1.216	49 ± 18.48	29.12 ± 2.325	1.609 ± 0.04
CCD1	0.038 ± 0.003	0.197 ± 0.003	0.131 ± 0.001	23.26 ± 0.819	666 ± 27.5	19.15 ± 1.711	1.402 ± 0.04
CCD2	0.029 ± 0.012	0.303 ± 0.005	0.164 ± 0.002	20.45 ± 0.74	772 ± 63.91	15.7 ± 1.812	1.197 ± 0.017
CCD3	0.057 ± 0.003	0.309 ± 0.004	0.176 ± 0.001	25.34 ± 0.868	317 ± 22.01	19.37 ± 1.909	1.24 ± 0.017
CCD4	0.051 ± 0.002	0.286 ± 0.007	0.186 ± 0.001	23.5 ± 0.745	437 ± 18.91	16.99 ± 1.799	1.207 ± 0.018
CCD5	0.041 ± 0.004	0.197 ± 0.002	0.122 ± 0.001	26.01 ± 1.048	508 ± 13.1	20.99 ± 1.878	1.434 ± 0.018
CCD6	0.033 ± 0.006	0.196 ± 0.003	0.189 ± 0.001	20.01 ± 1.86	751 ± 10.18	13.99 ± 1.986	1.221 ± 0.014
CCD7	0.055 ± 0.003	0.263 ± 0.002	0.121 ± 0.002	20.04 ± 0.841	873 ± 29.99	17.66 ± 1.802	1.626 ± 0.022
CCD8	0.053 ± 0.008	0.212 ± 0.007	0.202 ± 0.002	23.17 ± 0.737	230 ± 13.29	18.99 ± 1.451	1.263 ± 0.02
CCD9	0.032 ± 0.01	0.199 ± 0.009	0.177 ± 0.002	23.13 ± 0.726	429 ± 19.89	18.66 ± 1.571	1.231 ± 0.014
CCD10	0.033 ± 0.109	0.211 ± 0.008	0.179 ± 0.002	23.23 ± 0.725	442 ± 20.19	18.66 ± 1.57	1.23 ± 0.014
CCD11	0.03 ± 0.011	0.201 ± 0.01	0.177 ± 0.001	22.98 ± 0.715	445 ± 23.23	18.67 ± 1.569	1.22 ± 0.013
CCD12	0.032 ± 0.009	0.199 ± 0.011	0.181 ± 0.003	23.23 ± 0.712	417 ± 18.33	18.56 ± 1.569	1.21 ± 0.014
CCD13	0.039 ± 0.01	0.282 ± 0.008	0.176 ± 0.003	23.03 ± 0.726	427 ± 19.33	18.67 ± 1.574	1.2 ± 0.012

a, aa=Kawakita constant; b=Kuno constant; c=angle of repose; d=particle size; e= carr's index;
f= hausner's ratio *= All observations are shown in mean ±SD (n=3)

Table 2: b) Evaluation of experimental design batches*

Batch	CF[g]	IF[h]	YLD[i] (%)	CS[j]	AR[k]	SF[l]	DC[m] (%)
IRB	0.387 ± 0.0009	0.573 ± 0.012	100	-	7.98 ± 0.375	0.352 ± 0.016	100 ± 1.027
CCD1	0.999 ± -0.008	1.825 ± 0.105	80.35 ± 2.55	25.07 ± 0.085	1.071 ± 0.058	0.926 ± 0.001	96.82 ± 0.89
CCD2	1.069 ± 0.057	1.187 ± 0.056	88.8 ± 2.95	25.57 ± 0.034	1.067 ± 0.107	0.998 ± 0.031	98.68 ± 1.212
CCD3	1.162 ± 0.168	1.331 ± 0.194	89.89 ± 2.75	24.27 ± 0.088	1.126 ± 0.079	0.946 ± 0.074	93.18 ± 1.064
CCD4	1.136 ± 0.01	1.066 ± 0.125	81.78 ± 1.75	25.07 ± 0.019	1.077 ± 0.076	0.952 ± 0.008	97.93 ± 1.128
CCD5	1.845 ± 0.301	2.017 ± 0.305	90.69 ± 2.06	24.77 ± 0.053	1.145 ± 0.064	0.748 ± 0.063	96.18 ± 1.176
CCD6	1.045 ± 0.105	1.154 ± 0.083	92.49 ± 2.09	25.17 ± 0.074	1.034 ± 0.039	0.997 ± 0.055	96.43 ± 1.114
CCD7	1.271 ± 0.05	1.802 ± 0.194	89.25 ± 2.11	25.27 ± 0.115	1.168 ± 0.085	0.886 ± 0.002	98.43 ± 1.624
CCD8	1.137 ± 0.233	1.546 ± 0.222	88.61 ± 2.07	24.77 ± 0.019	1.16 ± 0.155	0.961 ± 0.105	97.18 ± 1.113
CCD9	1.105 ± 0.058	1.743 ± 0.167	88.42 ± 2.68	24.97 ± 0.057	1.085 ± 0.044	0.967 ± 0.03	96.68 ± 1.36
CCD10	1.101 ± 0.051	1.746 ± 0.161	88.22 ± 2.66	24.95 ± 0.054	1.068 ± 0.044	0.961 ± 0.031	97.08 ± 1.364
CCD11	1.111 ± 0.053	1.696 ± 0.168	88.18 ± 2.65	25.07 ± 0.049	1.088 ± 0.046	0.971 ± 0.032	96.13 ± 1.371
CCD12	1.091 ± 0.055	1.646 ± 0.166	88.6 ± 2.67	25.42 ± 0.048	1.058 ± 0.044	0.961 ± 0.03	97.17 ± 1.369
CCD13	1.101 ± 0.051	1.846 ± 0.164	87.77 ± 2.66	25.12 ± 0.047	1.078 ± 0.045	0.961 ± 0.029	96.03 ± 1.361

g=circularity factor; h=irregularity factor; i=yield; j=crushing strength; k=Aspect ratio; l=shape factor; m=drug content. *= All observations are shown in mean ±SD (n=3)

PRINCIPAL COMPONENT ANALYSIS

First, we used Principal Component Analysis (PCA) to investigate the key factors affecting the characteristics of the agglomerates. PCA, which breaks down results into latent variables or principal components that explain the main variance in the dataset, is well-known for its usefulness in revealing correlations among many variables [35]. Our first PCA examined the relationship between all characteristics obtained from spherical agglomeration studies and untreated IRB crystals. The first principal component (PC1) explained 100% of the variance in the dataset, as seen in Figure 2. PC1 showing 100% variation implies that all variables can be expressed as a linear transformation of a single variable, indicating an extreme case of linear dependence among the variables. Additionally, it might be from highly correlated data or a specific data structure where one component dominates [36]. Interestingly, the score plot showed that IRB was an outlier clearly defined outside the elliptical zone and isolated from the agglomerates of all 13 trials.

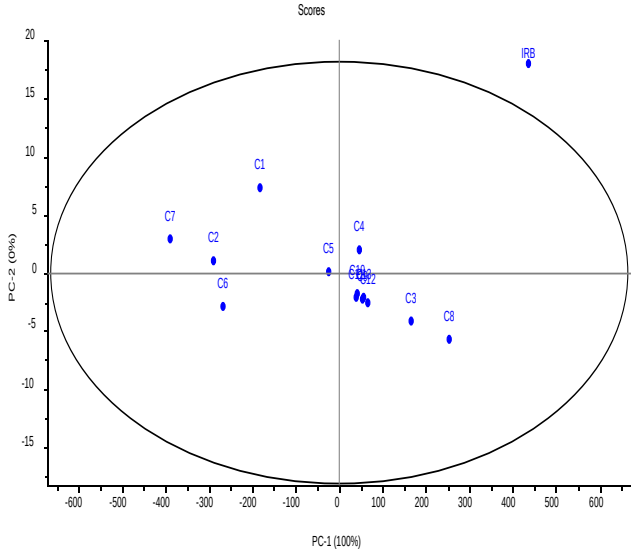

Figure 2: PCA Score Plot Comparing Prisitne and Agglomerated IRB Samples

The PCA score plot in Figures 3 and 4 shows the distribution of all 13 batches from the central composite design. The score plot shows that the batches are evenly distributed over the four quartiles and that the first principal component (PC1), which is 100%, accounts for all the dataset variability [37]. To evaluate the similarities and differences across the 13 trials, AHCA also divides them into discrete groups. Group I (C3 and C8), Group II (C4, C5, C9, C10, C11, C12, and C13), Group III (C1, C2, and C6), and Group IV (C7) are the groups of formulas shown in Figure 5. Interestingly, these groupings show a great deal of separation and dissimilarity.

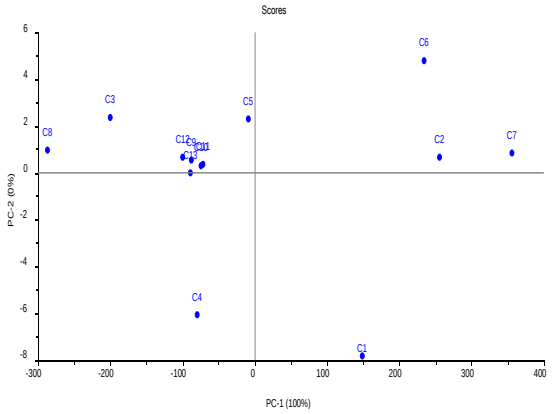

Figure 3: 2D Score Plot Agglomerated IRB Analysis Using PCA

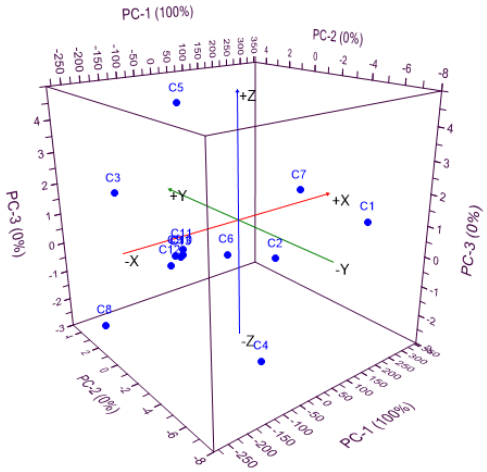

Figure 4: 3D Score Plot Agglomerated IRB Analysis Using PCA

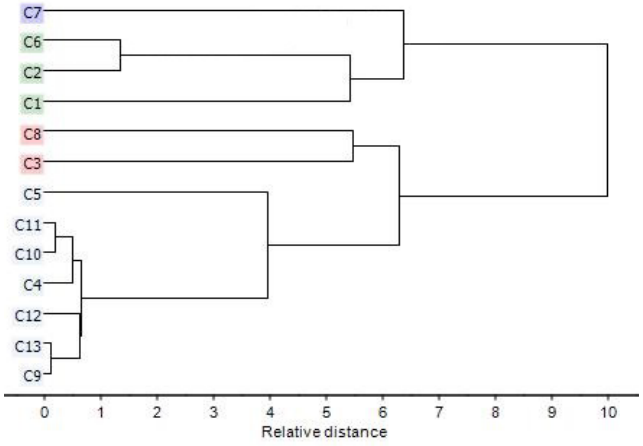

Figure 5: Agglomerated IRB Dendrogram: Unveiling Hierarchical Clustering Patterns

The loading plot representation for the first two primary components is shown in Figures 6 and 7. In loading plots, variables that are close to one another are typically viewed as positively correlated, whereas variables that are on opposite sides of the origin are interpreted as negatively linked [38].

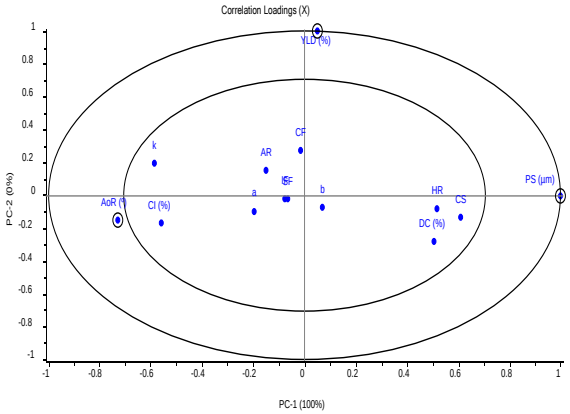

Figure 6: Innovative Visualization 2D Loading Plot from PCA Analysis of Agglomerated IRB

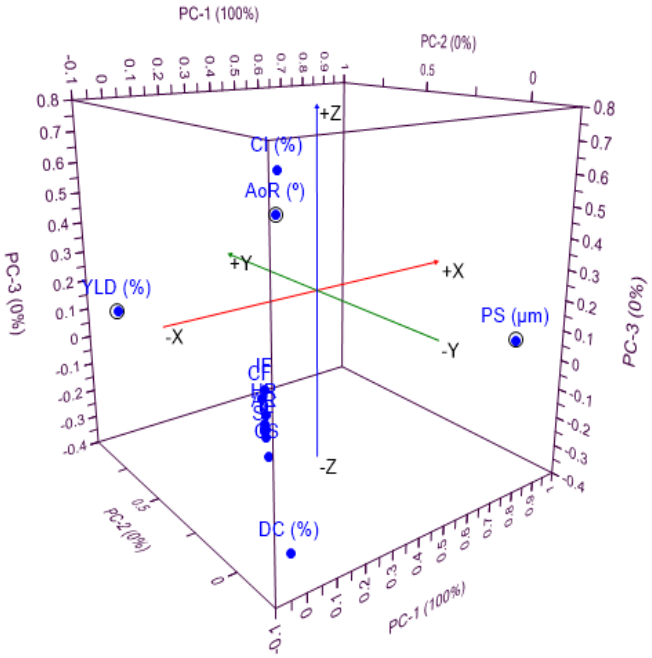

Figure 7: Innovative Visualization: 3D Loading Plot from PCA Analysis of Agglomerated IRB

A loading plot was created to determine the important factors for further optimization. Figure 6 shows the correlation loading plot, which shows the four most important variables as a circle surrounded by two ellipses [5,39]. After the study, it was determined that the variables AoR, PS, and YLD were important in forming spherical agglomerates. As a result, they were selected for additional optimization.

REGRESSION ANALYSIS

All 13 batches showed a significant variation in the dependent variables (AoR, PS, and YLD), which ranged from 20.01 to 26.01°, 230 µm to 873 µm, and 80.35% to 92.49%, respectively. This variation highlights how much X1 and X2 have an impact on these answers. Effective conclusions can be reached by looking at the polynomial equations and taking into account the magnitude and mathematical sign of the coefficients (whether positive or negative). Specifically, for AoR and PS, b12, b11, and b22 were excluded from the whole model since their p-values were more than 0.05, indicating that they were not significant. Likewise, b11 and b22 were removed for YLD for the same reason. The logic for excluding these unimportant factors is supported by the ANOVA findings shown in Table 3. AoR, PS, and YLD high correlation coefficients signify a good model fit. The AoR, PS, and YLD critical F values at $\alpha = 0.05$ were found to be 4.34 (df = 3, 7), 4.34 (df = 3, 7), and 4.74 (df = 2, 7), in that order. Additionally, it was discovered that the computed F values (0.434 for PS, 0.258 for YLD, and 4.084 for AoR) were less than the critical levels, suggesting that there was no discernible difference between the full and reduced models (Table 4).

Table 3: Irbesartan Spherical Crystals: Unveiling Insights through Regression Analysis

Coefficients	*AoR (Y_1)*		*YLD (Y_2)*		*PS (Y_3)*	
	FM [a]	***RM*** [b]	***FM***	***RM***	***FM***	***RM***
b_0	23.09	22.88	89.20	89.20	488.43	516.46
b_1 [c]	-1.64	-1.64	0.36	0.36	71.21	71.21
b_2 [d]	1.19	1.19	0.20	0.20	-199.17	-199.17
b_{12} [c, e]	0.24	-	-4.14	-4.14	3.50	-
b_{11} [c, e]	0.84	-	-7.85	-	87.61	-
b_{22} [c, e]	-0.79	-	3.86	-	-28.04	-

[a] FM, Full model; [b] RM, Reduced model; [c] Nonsignificant (P>0.05) coefficients for Y_1; [d] Nonsignificant (P>0.05) coefficients for Y_2; [e] Nonsignificant (P>0.05) coefficients for Y_3

The coefficients in Table 3 show the effects of factors (FM and RM) on response variables (AoR, YLD, and PS). The intercept (b0) demonstrates that FM has a somewhat higher baseline for AoR and PS than RM, although both start equally with YLD. FM had a negative effect on AoR (b1 = -1.64) but a good effect on YLD (b1 = 0.36) and PS (b1 = 71.21). In contrast, RM has an advantageous impact on AoR (b2 = 1.19) and YLD (b2 = 0.20) but a negative influence on PS (b2 = -199.17). Interaction effects (b12) have a synergistic effect on AoR (b12 = 0.24) and PS (b12 = 3.50) when FM and RM are both high. Nonlinear relationships are indicated by quadratic terms (b11 and b22): FM's squared effect positively influences AoR (b11 = 0.84) and PS (b11 = 87.61), but negatively affects YLD (b11 = -7.85), whereas RM's

squared effect negatively affects AoR (b22 = -0.79) and PS (b22 = -28.04). These coefficients shed light on how differences in FM and RM affect outcomes, revealing their practical relevance for optimizing procedures in the study. Using Design Expert software version 13, interpolated values were obtained from the data collected across 13 batches. The analysis showed that while YLD was higher, the ideal concentrations of X1 and X2 were linked to lower AoR and PS values. Further evidence of negative coefficients (b1) for AoR was provided by multiple linear regression analysis (see Table 3), which suggested that an increase in talc content would decrease the angle of repose. On the other hand, higher talc concentration results in larger agglomerates and higher yields, as indicated by positive coefficients (b1) for PS and YLD. Reduced agitation speed also increases PS and flowability but decreases YLD, according to negative coefficients (b2) for PS and positive coefficients for AoR and YLD.

Table 4: Calculation of testing the models in portions

Model	*df* [c]	*SS* [d]	*MS* [e]	R^2
Angle of Repose (Y_1)				
Regression				
FM[a]	5	37.039	7.408	0.9495
RM[b]	2	32.983	16.491	0.8455
Residual				Fcal = 4.084
FM	7	1.970	0.281	Fcritical = 4.35
RM	10	6.026	0.603	df = (3, 7)
Yield (Y_2)				
Regression				
FM	5	112.842	22.568	0.8591
RM	3	111.475	37.158	0.8487
Residual				Fcal = 0.258
FM	7	18.513	2.645	Fcritical = 4.74
RM	9	19.879	2.209	df = (2, 7)
Particle Size (Y_3)				
Regression				
FM	5	369888.351	73977.670	0.852
RM	2	357904.335	178952.167	0.824
Residual				Fcal = 0.434
FM	7	64328.880	9189.840	Fcritical = 4.35
RM	10	76312.896	7631.290	df = (3, 7)

[a]FM, Full model; [b]RM, Reduced model; [c] df, Degree of freedom; [d] SS, Sum of squares; [e] MS, Mean of squares

As the amount of talc increases, the X2 coefficient (1.19) on AoR shows a positive effect, demonstrating a direct association. Agglomerate fracture caused by faster speeds lessens sphericity and flow characteristics. Figure 8's contour and response surface plots as well as Figure 9a's perturbation plot make this link clear. The following is the polynomial equation that was obtained via regression analysis:

$AoR = 23.09 - 1.64X_1 + 1.19X_2 + 0.84X_1^2 - 0.79X_2^2 + 0.24X_1X_2$ (Eq. 12)

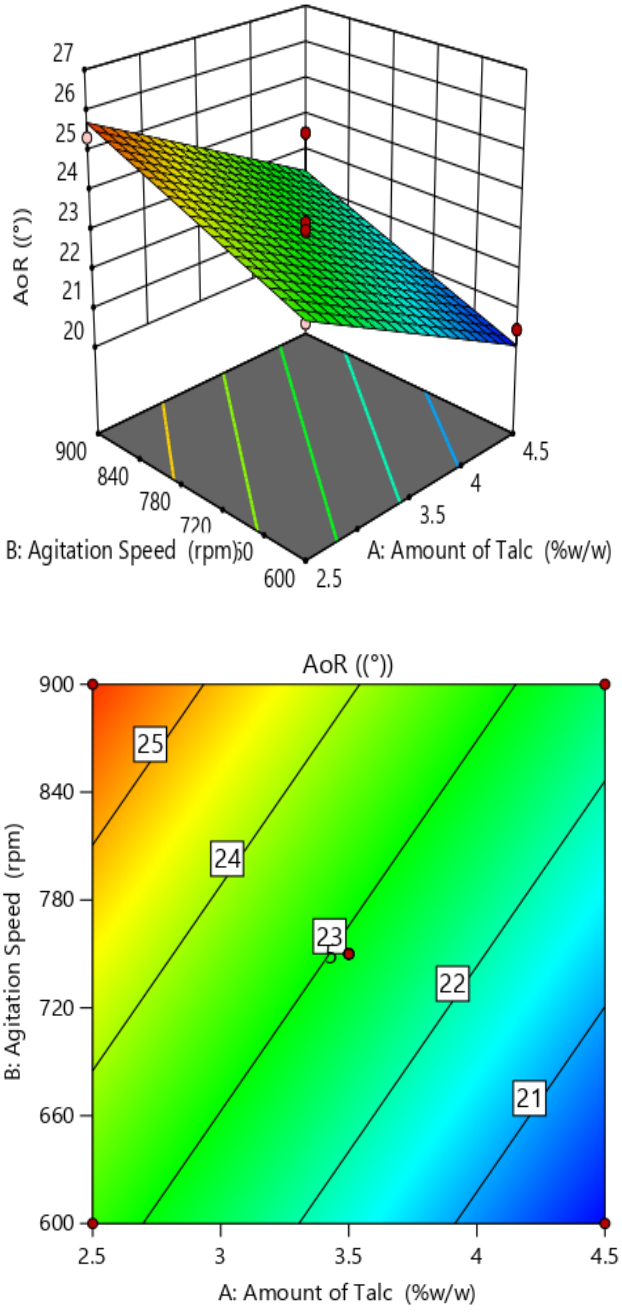

Figure 8: Analyzing AoR variations with talc amount and agitation speed via contour and response surface plot

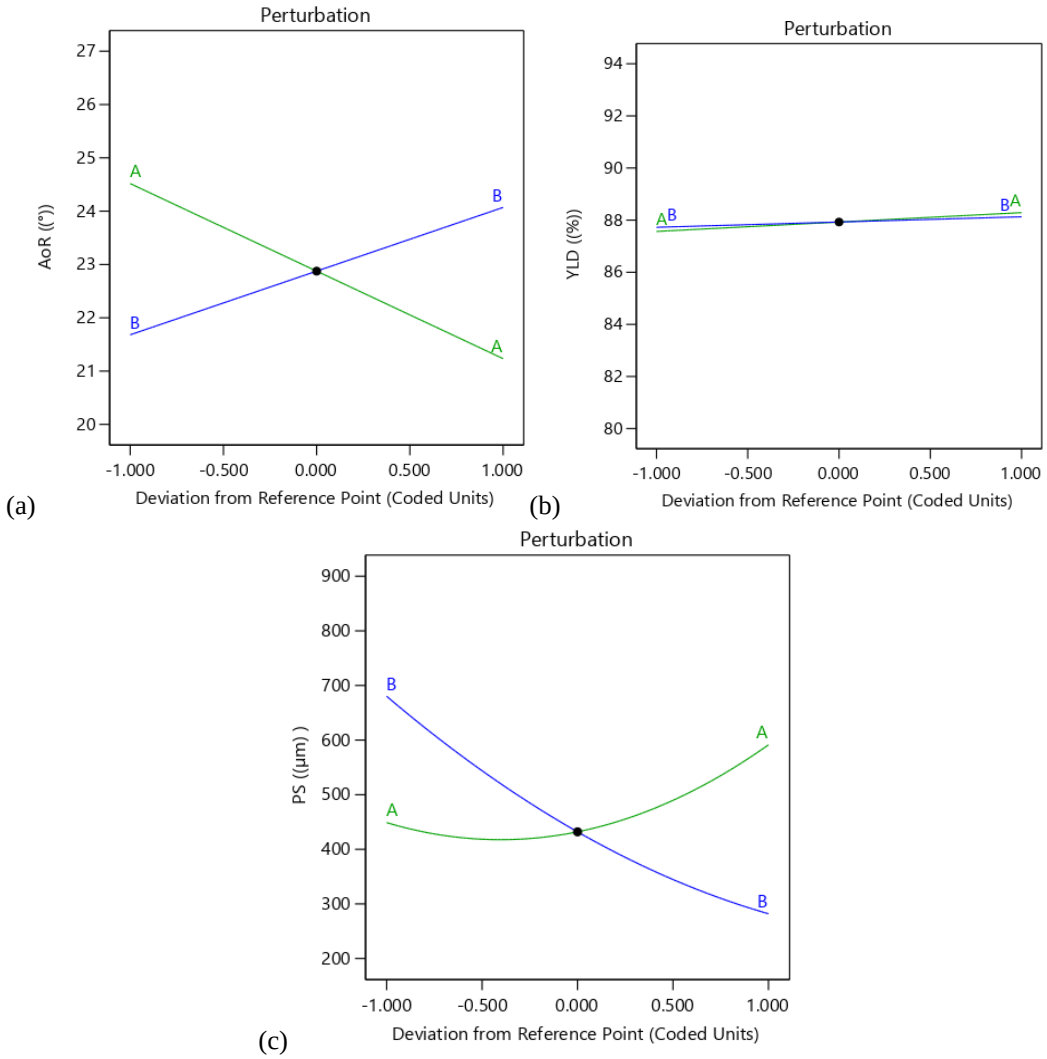

Figure 9 Perturbation plot: Impact on a) AoR, b) YLD, and c) PS

Influence of variables on YLD

When YLD was examined in relation to variable X1 (talc percentage), it was found that YLD varied between 80.35% and 92.49% for each of the 13 formulations. In CCD1, the lowest YLD was noticeable. Variable X1 has a positive coefficient (0.36), indicating that it has a positive impact on YLD. The perturbation analysis of YLD indicates that factor X2 deviates from X1 at different levels, suggesting that X2 has less of an impact on YLD. Contour and response surface graphs showing YLD against talc %, agitation speed, and perturbation (Figure 10; Figure 9b) corroborate this observation. Additionally, the following polynomial equation was created using regression analysis:

$$YLD = 89.20 + 0.36X_1 + 0.20X_2 - 7.85X_1^2 + 3.86X_2^2 - 4.14X_1X_2 \quad \text{(Eq. 13)}$$

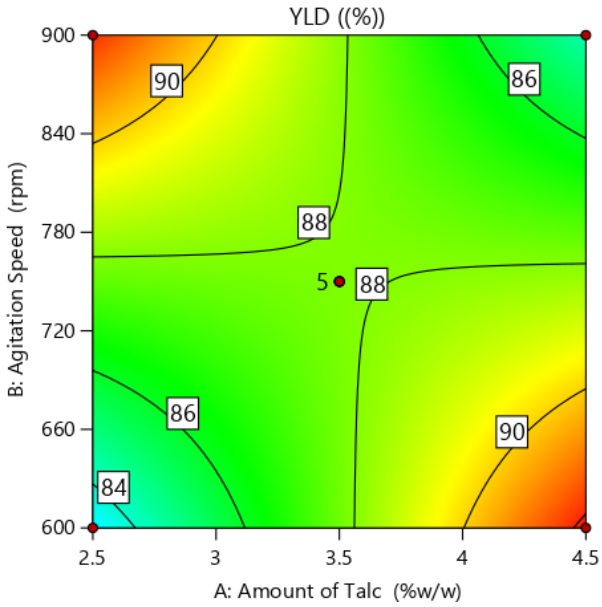

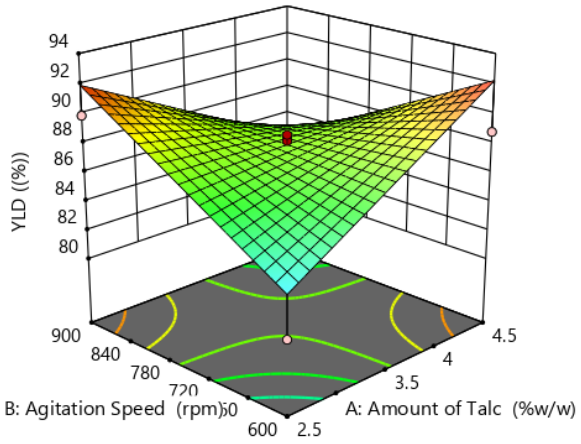

Figure 10: Analyzing yield variations with talc amount and agitation speed via contour and response surface plot

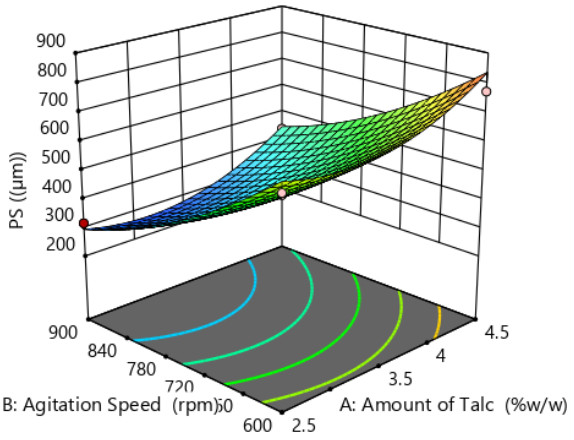

Figure 11: Analyzing Particle Size variations with talc amount and agitation speed via contour and response surface plot

Influence of variables on PS

The distribution of particle size (PS) is broad, and these factors notably impact the agglomeration size. The variable X1's positive coefficient (71.21) suggests a significant relationship between PS and the amount of talc. This may be explained by the talc's ability to absorb crystals, increasing the agglomerates' deformable structure and size. On the other hand, the negative coefficient (-199.17) for X2 indicates that PS falls with increasing agitation speed. Increased agitation speeds cause agglomerates to become disrupted, reducing particle size and increasing fine production. Contour and response surface plots showing PS against talc quantity and agitation speed (Figure 11) corroborate these conclusions. The Perturbation plot of PS (Figure 9c) offers additional corroboration, supporting the previously stated findings. Furthermore, the following polynomial equation is provided, which was obtained by regression analysis:

$PS=488.43+71.21X_1–199.17X_2+87.61X_1^2–28.04X_2^2+3.50X_1X_2$ (Eq. 14)

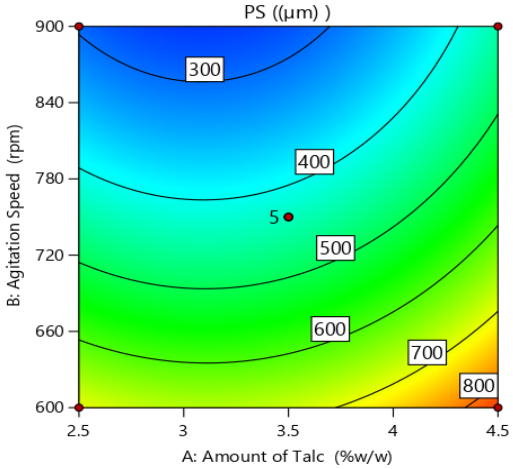

OPTIMIZATION OF AGGLOMERATES

The following standards were used to choose the best formulation: I. Reaching the lowest Angle of Repose (AoR) value, II. Ensure that the particle size (PS) value is within the designated range and III. Reaching the maximum Yield (YLD) value. The CCD procedure yielded the optimized formulation, whose composition and expected response results are in Table 5. In Figure 12, the matching overlay plot is shown. The optimized batch of spherical agglomerates was made by the software's suggested factor levels to validate the design. Table 5 compares the experimental and projected values, showing minimal percent relative errors and verifying the model's goodness of fit [13].

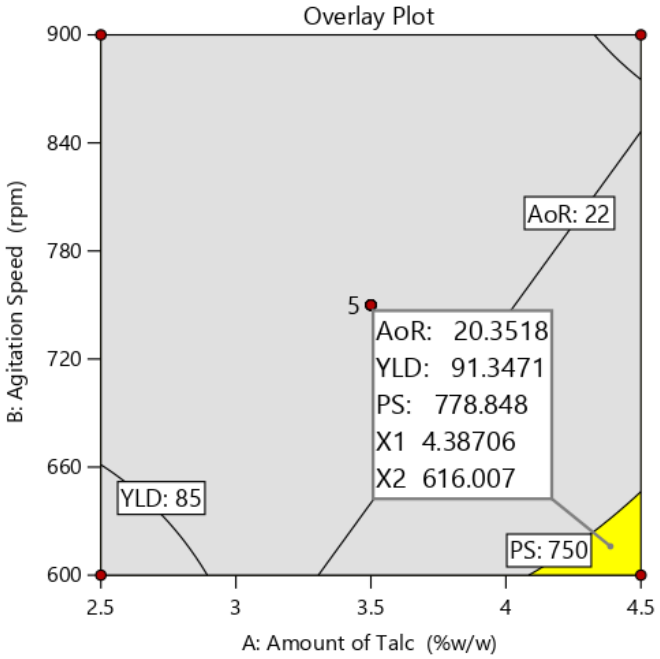

Figure 12: Visualization of Checkpoint batch: Overlay Plot Analysis

Table 5. Performance evaluation of optimized irbesartan spherical crystals

Response	*Predicted Value*	*Experimental Value [Mean ± SD (n=3)]*	*% Relative Error*
AoR (°)	20.35	21.24 ± 1.03	-4.19%
YLD (%)	91.35	88.71 ± 2.55	2.98%
PS (µm)	778.84	752.41 ± 24.73	3.51%

EVALUATION OF EXPERIMENTAL DESIGN BATCH

Drug content

Table 2 shows the data for the drug content analysis of spherical agglomerate. All the prepared agglomerate batches contained IRB within the limit as per USP. Using these values, the amount of SC containing IRB equivalent to 100 mg was calculated and probed for the drug release study.

Kawakita and Kuno analysis

All experimental design batches were found to have good flowability and densification, with values of "a" smaller than "b." Figure 13 displays the Kawakita analysis plot. Table 2 lists the values of the Kawakita constants "a" and "b." The value of "a" was substantially lower than the value of IRB for every design batch, showing superior agglomeration flowability [40]. The larger value of "b" has been observed to contribute to the higher compressibility of agglomerates. Because the agglomerates had superior flow and packability, they were packed more densely even without tapping, as seen by the apparent packing velocity achieved by tapping (represented by parameter b) for the agglomerates compared to the IRB [41].

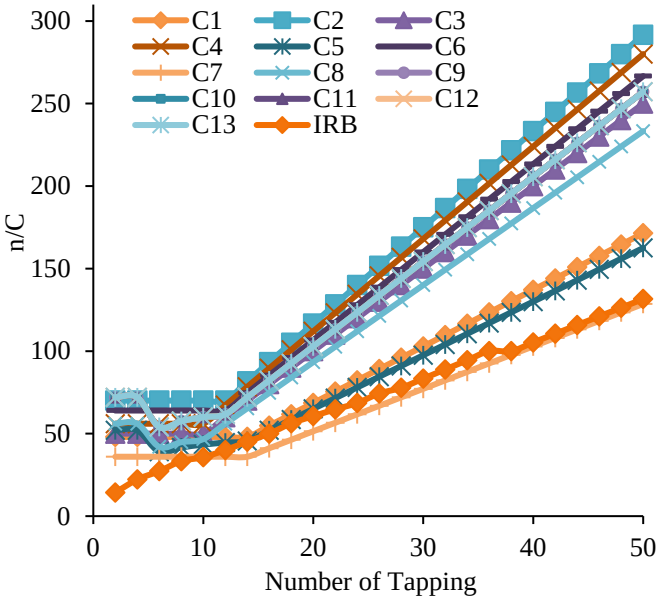

Figure 13: Kawakita analyses of design batches

These results were validated by the greater "k" of Kuno analysis obtained for the agglomerates. A linear decrease in the volume of the solid bed with the tappings confirmed the poor packability of IRB [42], whereas packability was comparatively poor for agglomerates (b = 0.025 ± 0.0008). The rate of change of n/C due to tapings was found to be 4.97 ± 0.312 for IRB, which is quite less than agglomerates. A higher packing process rate is associated with a larger value of "k" in the Kuno analysis for spherical agglomerates (Figure 14).

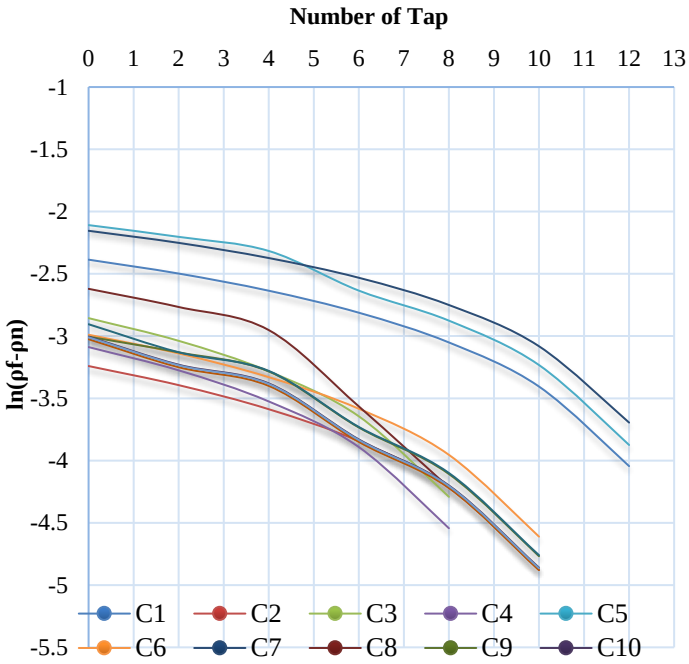

Figure 14: Kuno analyses of design batches

Surface topography and sphericity determination

For the surface topography and sphericity determination SF, CF, IF and AR was calculated. Results obtained from this were shown in Table 2. The microscopic images of IRB agglomerates are given in Figure 15. The SF results show that all the design batches have good SF value which is near to 1. As perfect round shape has SF value 1 all the batches has value closest to 1 [5]. IRB has SF value 0.352, interpret that it is totally irregular in shape. The CF value also near to one shows good sphericity. It also referred as roundness value. The aspect ratio is ratio of maximum dimeter of particle to the diameter measured right angle to it. As the aspect ratio is 1 for spherical shaped particles, perfect elliptical particles have AR 0 [14]. The results obtained were in 1.034 to 1.168 which shows that are particles are more spherical in shape rather than elliptical. Elongation causes the value of IF to decrease, whereas irregularities cause an increase in this value [43].

Figure 15: Microscopic images of optimized agglomerates

Flow properties of agglomerates

For design batches, PS, AoR, HR, and CI were computed; the results are displayed in Table 2. The PS for each batch was determined to be between 230 and 873 µm, and the AoR falls between 20.01 and 26.01. A low value of AoR indicates good agglomeration flow. Poor powder flow was indicated by the AoR score of 44.23 for the IRB [44]. AoR results corroborate the sphericity determination result since spherical shapes have good flowability [45]. The ranges of HR and CI, respectively, were found to be 1.197 to 1.626 and 13.991 to 20.986%. Agglomerates have higher HR and CI values than IRB, which suggests good flowability. These data support the conclusions of AoR and sphericity determination.

EVALUATION OF OPTIMIZED AGGLOMERATES

Three dependent variables were assessed for the checkpoint batch (i.e., AoR, PS, and YLD). Table 5 displays the outcome and the deviation from the expected value. The following are additional optimized batch evaluations:

Heckel analysis

To determine the compression characteristics of the agglomerated crystals, Heckel's equation was used to analyze the compression behavior of agglomerated crystals. The slope of Heckel plot 'K' indicates the plastic behavior of the material. The larger the value of 'K,' the greater the plasticity in the material [45]. The linearity in the graph (Figure 16) was an indication of plastic deformation. Moreover, the 'A' value of prepared agglomerates was less than that of pure drugs. This finding suggested that low compression pressure was required to obtain the closest packing of the spherical agglomerates, fracturing its texture and densifying the fractured particle [46]. The low value of yield strength was again an indication of low resistance to pressure, good densification, and easy compaction [23]. Thus, the Heckel plot suggested that agglomerated crystals showed an ease of fracture. This created new crystal surfaces that might have made plastic deformation during compression easier [47].

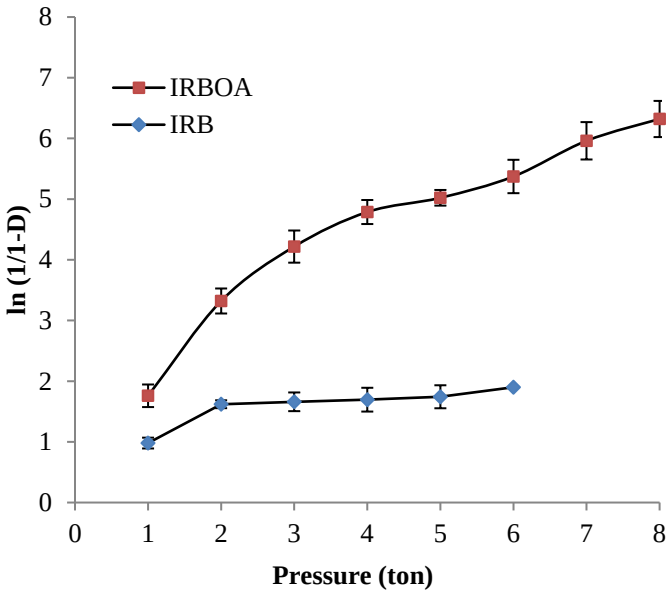

Figure 16: Heckel plot of IRB and optimized agglomerates (IRBOA)

Elastic recovery

Reduced elastic recoveries of spherical agglomerates compared to pure drugs indicated the possibility of agglomerates breaking easily, and the creation of additional surfaces may have encouraged plastic deformation under compression [48].

Fourier transform infrared (FTIR) spectroscopy

Compatibility studies were performed using an FT-IR spectrophotometer. The IR spectrum of pure drug and prepared spherical agglomerates by making a KBr disc. The characteristic absorption peaks of IRB were obtained at different wave numbers. The peaks obtained in the prepared spherical agglomerates' spectra correlate with the drug spectrum's peaks. This indicates that the drug is compatible with the formulation components [49]. The spectra for pure drug and optimized formulations are shown in Figure 17. Pure IRB spectra showed sharp characteristic peaks at 3390.69 cm^{-1}, 2968.97 cm^{-1}, 1739.86 cm^{-1}, 1676.57 cm^{-1}, and 1623.91 cm^{-1}. FTIR-spectra of IRB and its physical mixtures with excipients are the same, and there is no significant shift of peaks or disappearance of principle peaks or modification of the principle peaks, indicating no interaction between the drug and excipients [50].

Differential Scanning Calorimetry (DSC)

Dependable information about the physicochemical state of the spherical agglomerates and potential interactions between the drug and polymer can be obtained using differential scanning

calorimetry. DSC validated the homogeneity of the crystalline structure in the optimized batch, demonstrating that the drug's melting point was unaffected by the use of HPMC K4M, PVP K30, and talc in the crystallization of IRB. Every sample had a sharp melting point and a flat baseline, indicating that hydration, salvation, and polymorphic transitions had not happened during the particle's crystallization [46]. A distinctive, prominent exothermic peak indicates the drug's crystalline nature at 182°C on the IRB DSC thermogram (Figure 18). This peak is linked to the drug's melting point.

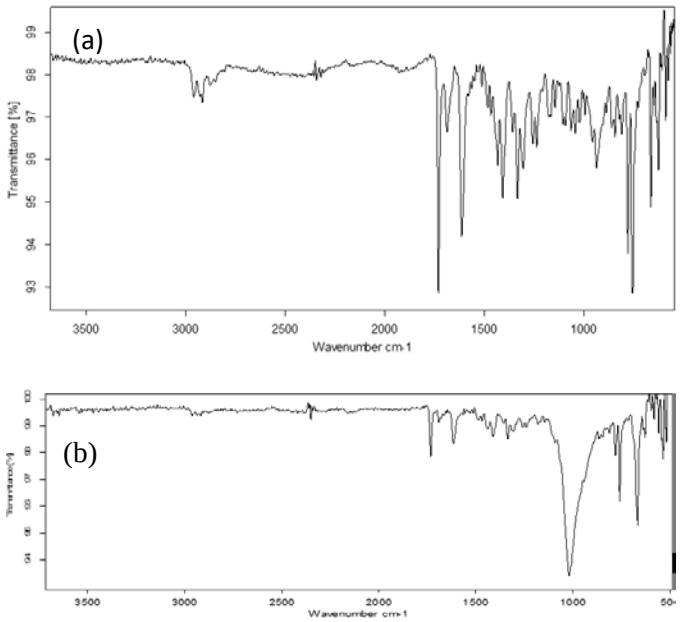

Figure 17 FTIR spectra of (a) Pure drug IRB; (b) optimized IRB agglomerates

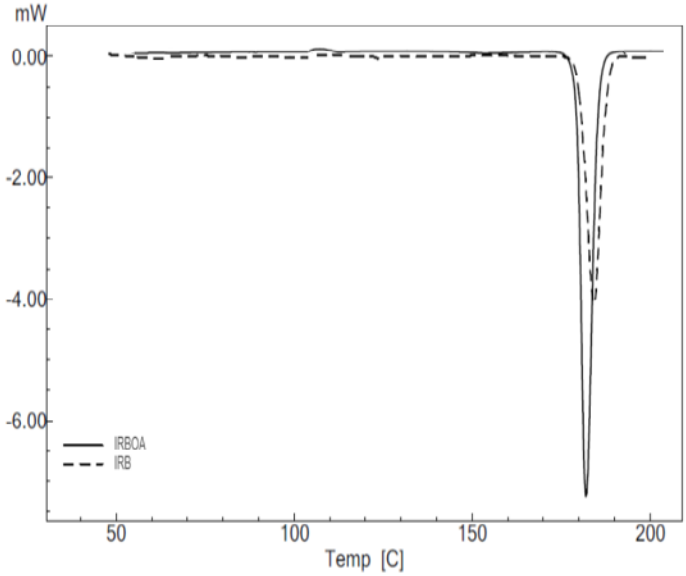

Figure 18 DSC thermogram of pure IRB and optimized agglomerates (IRBOA)

X-Ray Powder Diffraction (XPRD)

As seen in Figure 19, the X-ray diffraction pattern of IRB showed strong, intense, and less diffused peaks confirming the drug's crystalline structure. At 2θ degrees, it was evident that there are diffraction peaks at 12.9, 14.7, 16.4, 17.9, 21.3, and 21.9. However, the IRB and its agglomerate x-ray diffraction patterns were the superimposition of each component about the IRB peaks; only the relative intensity at the 2θ angle of these peaks stayed essentially the same. Measurements of the crystallinity index were made to assess the crystal character loss [51]. The crystallinity index is the greatest peak height in the formulation's XRD divided by the maximum peak height in pure IRB [11]. It has the symbol Ci. Agglomerates were discovered by Ci at 0.223. It shows that 74% of pure IRB still has its crystalline behavior. It implies that the substance underwent amorphization [52]. X-ray diffractometry validates the notion supported by IR and DSC tests.

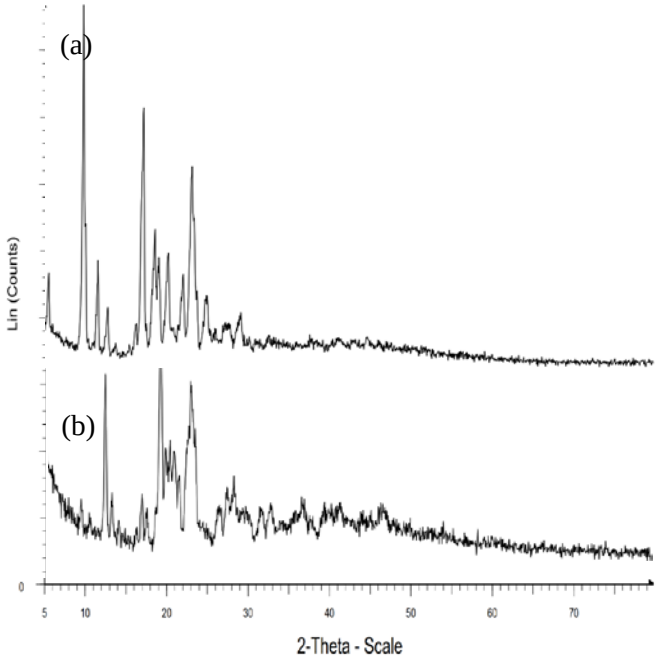

Figure 19 X-Ray diffraction spectra of (a) pure IRB; (b) optimized IRB agglomerates.

Scanning Electron Microscopy (SEM)

Figure 20 shows a scanning electron micrograph of a produced spherical crystal and a pure drug. Whereas IRB agglomerates were spherical, pure IRB displayed a rod-shaped crystal habit. The picture graph demonstrated that the agglomerates formed were spherical and had a rough surface due to the IRB crystal cluster that formed them.

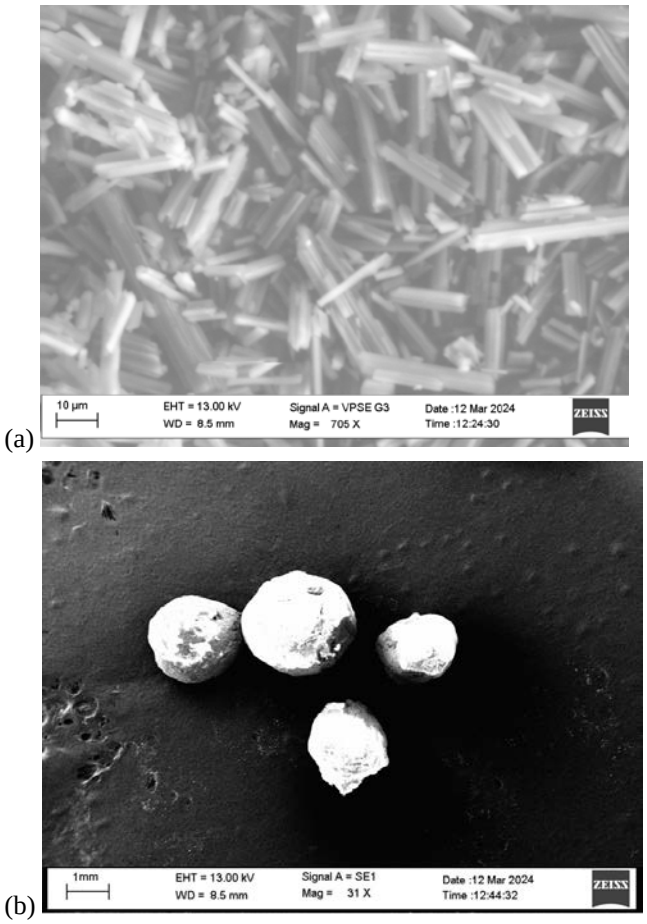

(a)

(b)

Figure 20: Scanning electron microscopic image of Pure IRB (a) and Optimized IRB agglomerates (b)

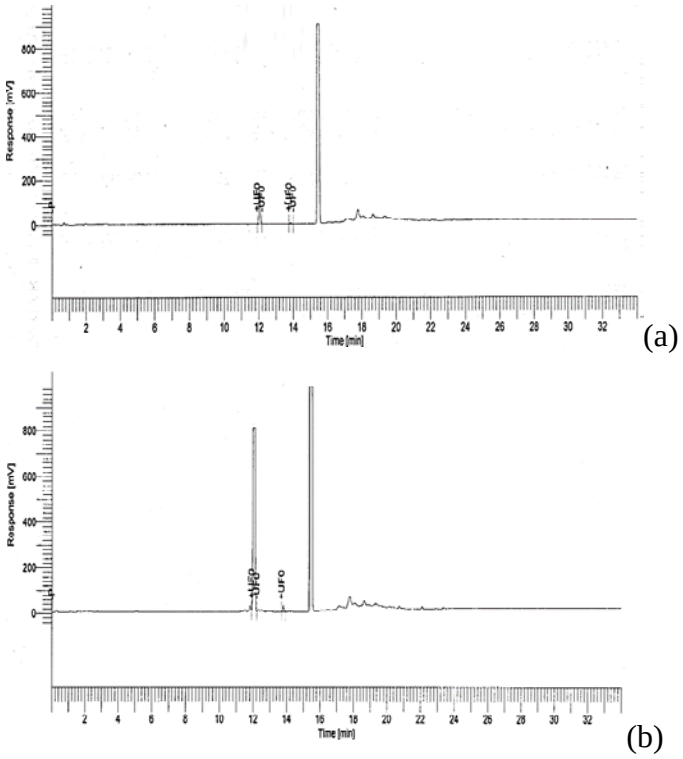

(a)

(b)

Figure 21: GC spectra of formulation (a) sample run; (b) standard run

Gas chromatography (GC)

A DMF and toluene GC analysis of the agglomeration was carried out to determine the residual solvents. The amount of DMF and toluene per 150 mg agglomerates was calculated by the following formula:

$$PDE = \frac{Dose \times Concentration}{1000} \qquad \text{(Eq. 15)}$$

Agglomerates contained 16.27 ppm of DMF and 11.41 ppm of toluene, respectively. Toluene and DMF have respective limits of 880 ppm and 820 ppm. This demonstrates that the formulation exceeded the organic volatile impurity limitations and may not harm humans [53,54]. Figure 21 displays the formulation's GC spectra.

STABILITY STUDY OF AGGLOMERATES

Agglomerates were subjected to a further evaluation of stability after a month. Table 6 displays the AoR, CS, and PS results. The results confirm the formulation's stability, indicating that the formulations held together during the stability testing.

Table 6: Stability parameters of optimized agglomerates of IRB

Parameters	Before stability	After stability
AoR (°)	21.24 ± 1.03	21.56 ± 0.94
PS (µm)	752.41 ± 24.73	742.59 ± 19.42
CS (gm)	34.67 ± 3.31	36.21 ± 4.07

CONCLUSION

This study demonstrates the effective application of spherical crystallization for optimizing the micromeritic properties of irbesartan. By integrating crystallization and agglomeration techniques, spherical agglomerates were successfully produced without additional granulation steps. Key parameters such as stirring rate, bridging liquid quantity, and polymer concentration were meticulously adjusted to enhance particle size distribution and mechanical properties. Principal component analysis and central composite design facilitated identifying and optimizing critical parameters affecting product quality. Optimized agglomerates were found with an amount of talc at 4.38 %w/w and an agitation speed of 616 rpm. SEM analysis confirmed the agglomerates' desired sphericity (shape factor near to 1), while GC analysis ensured appropriate solvent levels were maintained. PXRD data indicated no polymorphic changes, and DSC/FTIR

analyses validated compatibility between excipients and the active pharmaceutical ingredient. The improved mechanical strength and compression characteristics underscore the efficacy of spherical crystallization as a promising method for enhancing the micromeritic attributes of irbesartan, offering novel insights and potential applications in pharmaceutical formulation.

FINANCIAL ASSISTANCE
Nil

CONFLICT OF INTEREST
The authors declare no conflict of interest

AUTHOR CONTRIBUTION
V. D. Gorde led the research conceptualization, methodology design, and experimental validation, ensuring the study's scientific rigor. Punit R. Rachh contributed significantly to data analysis and interpretation using Principal Component Analysis (PCA) and experimental design techniques. Someshwar Mankar provided critical insights into the findings' pharmaceutical aspects and practical applications. Saurin Amin assisted with statistical analysis and optimization, enhancing the study's accuracy and reliability.

REFERENCES
[1] Arabi JH, Subramanian L, Rajesh M. A review on spherical crystallization: a novel technique in the field of particle engineering. *World Journal of Biology Pharmacy and Health Sciences*, **13(1)**, 78–93 (2023).

[2] Kawashima Y. Development of spherical crystallization technique and its application to pharmaceutical systems. *Archives of Pharmacal Research*, **7(2)**, 145–151 (1984).

[3] Garala KC, Patel JM, Dhingani AP, Dharamsi AT. Preparation and evaluation of agglomerated crystals by crystallo-co-agglomeration: an integrated approach of principal component analysis and Box–Behnken experimental design. *International Journal of Pharmaceutics*, **452(1–2)**, 135–156 (2013).

[4] Shangraw RF. Compressed tablets by direct compression. *Pharmaceutical Dosage Forms: Tablets*, **1**, 195–246 (1989).

[5] Garala KC, Patel JM, Dhingani AP, Dharamsi AT. Quality by design (QbD) approach for developing agglomerates containing racecadotril and loperamide hydrochloride by crystallo-co-agglomeration. *Powder Technology*, **247**, 128–146 (2013).

[6] Chattoraj S, Sun CC. Crystal and particle engineering strategies for improving powder compression and flow properties to enable continuous tablet manufacturing by direct compression. *Journal of Pharmaceutical Sciences*, **107(4)**, 968–974 (2018).

[7] Rojas J, Buckner I, Kumar V. Co-processed excipients with enhanced direct compression functionality for improved tableting performance. *Drug Development and Industrial Pharmacy*, **38(10)**, 1159–1170 (2012).

[8] Mohan S. Compression physics of pharmaceutical powders: a review. *International Journal of Pharmaceutical Sciences and Research*, **3(6)**, 1580–1592 (2012).

[9] Negro R. Endothelial effects of antihypertensive treatment: focus on irbesartan. *Vascular Health and Risk Management*, **4(1)**, 89 (2008).

[10] Pangarkar P, Thenge R, Mahajan N, Adhao V, Ajmire P. Crystal modification of irbesartan in presence of additive. *Journal of Advanced Pharmacy Education & Research*, **4(1)**, 106 – 113 (2014).

[11] Patel J, Dhingani A, Garala K, Raval M, Sheth N. Quality by design approach for oral bioavailability enhancement of irbesartan by self-nanoemulsifying tablets. *Drug Delivery*, **21(6)**, 412–435 (2014).

[12] Katta J, Rasmuson ÅC. Spherical crystallization of benzoic acid. *International Journal of Pharmaceutics*, **348(1–2)**, 61–69 (2008).

[13] Garala K, Joshi P, Shah M, Ramkishan A, Patel J. Formulation and evaluation of periodontal in situ gel. *International Journal of Pharmaceutical Investigation*, **3(1)**, 29 (2013).

[14] Raval MK, Garala KC, Patel JM, Parikh RK, Sheth NR. Functionality improvement of Chlorzoxazone by crystallo-co-agglomeration using multivariate analysis approach. *Particulate Science and Technology*, **39(6)**, 689–711 (2021).

[15] Davidson MW, Abramowitz M. Optical microscopy. Encyclopedia of Imaging Science and Technology, 2 (1106–1141), 120 (2002).

[16] Islam SF, Hawkins SM, Meyer JL, Sharman AR. Evaluation of different particle size distribution and morphology characterization techniques. *Additive Manufacturing Letters*, **3**, 100077 (2022).

[17] Al-Hashemi HMB, Al-Amoudi OSB. A review on the angle of repose of granular materials. Powder Technology, 330, 397–417 (2018).

[18] Tapas A, Kawtikwar P, Sakarkar D. An improvement of micromeritic properties and dissolution behaviors of carvedilol spherical agglomerates crystallized in presence of inutec SP1. *Turkish Journal of Pharmaceutical Sciences*, **9**, 101–112 (2012).

[19] Amidon GE, Secreast PJ, Mudie D. Particle, powder, and compact characterization. In Developing Solid Oral Dosage Forms (pp. 163–186). Elsevier (2009).

[20] Shah MK. Evaluation of physical and mechanical properties of Ibuprofen tablets using different bulking agents by means of Heckel and Kawakita Plots. Long Island University, The Brooklyn Center (2017).

[21] Patel RD, Raval MK, Sheth NR. Formation of Diacerein–fumaric acid eutectic as a multi-component system for the functionality enhancement. *Journal of Drug Delivery Science and Technology*, **58**, 101562 (2020).

[22] Haware RV, Tho I, Bauer-Brandl A. Evaluation of a rapid approximation method for the elastic recovery of tablets. *Powder Technology*, **202(1–3)**, 71–77 (2010).

[23] Garala K, Patel J, Patel A, Raval M, Dharamsi A. Influence of excipients and processing conditions on the development of agglomerates of racecadotril by crystallo-co-agglomeration. *International Journal of Pharmaceutical Investigation*, **2(4)**, 189 (2012).

[24] Shaha D, Sorathiab K. Design and evaluation of sustained release spherical agglomerates of Fluvastatin sodium by crystallo-co-agglomeration. *Journal of Applied Pharmaceutical Science*, **7(9)**, 99–108 (2017).

[25] Toufouki S, Ali A, Wang Y, Li R, Cao Y, Yao S. Deep eutectic solvents formed by pharmaceutical ingredients and their potential influences on solid preparations. *Journal of the Serbian Chemical Society*, **89(1)**, 107 – 121 (2023).

[26] Chandrasekharan S, Chinnasamy G, Bhatnagar S. Sustainable phyto-fabrication of silver nanoparticles using Gmelina arborea exhibit antimicrobial and biofilm inhibition activity. *Scientific Reports*, **12(1)**, 156 (2022).

[27] Madhvi K, Mehta K, Vadalia K, Jay C, Sandip K. Design and development of co-processed excipients for fast dissolving tablets of Irbesartan by melt agglomeration technique. *Journal of Pharmaceutical Investigation*, **45(2)**, 163–186 (2015).

[28] Bonetto RD, Ladaga JL, Ponz E. Measuring surface topography by scanning electron microscopy. II. Analysis of three estimators of surface roughness in second dimension and third dimension. *Microscopy and Microanalysis*, **12(2)**, 178–186 (2006).

[29] Shim H, Sah H. Assessment of residual solvent and drug in PLGA microspheres by derivative thermogravimetry. *Pharmaceutics*, **12(7)**, 626 (2020).

[30] Kumar M, Mandal UK. In-vitro Dissolution Study of Pharmaceutical Products with USP Apparatus-IV. *Drug Delivery Letters*, **11(3)**, 195–202 (2021).

[31] Usha AN, Mutalik S, Reddy MS, Ranjith AK, Kushtagi P, Udupa N. Preparation and, in vitro, preclinical and clinical studies of aceclofenac spherical agglomerates. *European Journal of Pharmaceutics and Biopharmaceutics*, **70(2)**, 674–683 (2008).

[32] Klevan I, Nordström J, Tho I, Alderborn G. A statistical approach to evaluate the potential use of compression parameters for classification of pharmaceutical powder materials. *European Journal of Pharmaceutics and Biopharmaceutics*, **75(3)**, 425–435 (2010).

[33] Maghsoodi M. Effect of process variables on physicomechanical properties of the agglomerates obtained by spherical crystallization technique. *Pharmaceutical Development and Technology*, **16(5)**, 474–482 (2011).

[34] Parasuraman S, Sujithra J, Syamittra B, Yeng WY, Ping WY, Muralidharan S, et al. Evaluation of sub-chronic toxic effects of petroleum ether, a laboratory solvent in Sprague-Dawley rats. *Journal of Basic and Clinical Pharmacy*, **5(4)**, 89–97 (2014).

[35] Turgeon M, Oualkacha K, Ciampi A, Miftah H, Dehghan G, Zanke BW, et al. Principal component of explained variance: an efficient and optimal data dimension reduction framework for association studies. *Statistical Methods in Medical Research*, **27(5)**, 1331–1350 (2018).

[36] Balasubramanian P, Praharaj PT. Principal component analysis revealed the key influencing factors of kombucha bacterial cellulose yield and productivity. *Bioresource Technology Reports*, **23**, 101539 (2023).

[37] Ivosev G, Burton L, Bonner R. Dimensionality reduction and visualization in principal component analysis. *Analytical Chemistry*, **80(13)**, 4933–4944 (2008).

[38] Popovicheva O, Padoan S, Schnelle-Kreis J, Nguyen D-L, Adam T, Kistler M, et al. Spring aerosol in urban atmosphere of megacity: analytical and statistical assessment for source impacts. *Aerosol and Air Quality Research*, **20(4)**, 702–717 (2020).

[39] Patel RD, Raval MK, Bagathariya AA, Sheth NR. Functionality improvement of Nimesulide by eutectic formation with nicotinamide: Exploration using temperature-composition phase diagram. *Advanced Powder Technology*, **30(5)**, 961-73 (2019)

[40] Patel RD, Raval MK, Pethani TM, Sheth NR. Influence of eutectic mixture as a multi-component system in the improvement of physicomechanical and pharmacokinetic properties of diacerein. *Advanced Powder Technology*, **31(4)**, 1441-56 (2020)

[41] Raval MK, Vaghela PD, Vachhani AN, Sheth NR. Role of excipients in the crystallization of Albendazole. *Advanced Powder Technology*, **26(4)**, 1102-15 (2015).

[42] Shelke M, Godge R, Sahane T, Pawar O, Kasar S. Stability Indicating RP-HPLC Method for Estimation of Cariprazine Hydrochloride in Human Plasma. *J. Appl. Pharm. Res.*, **12 (2)**, 27-34 **(**2024).

[43] Tay JYS, Liew CV, Heng PWS. Powder flow testing: judicious choice of test methods. *AAPS PharmSciTech*, **18**, 1843-54 (2017)

[44] Goh HP, Heng PWS, Liew CV. Comparative evaluation of powder flow parameters with reference to particle size and shape. *International Journal of Pharmaceutics*, **547 (1-2)**, 133-41 (2018)

[45] Raval MK, Sorathiya KR, Chauhan NP, Patel JM, Parikh RK, Sheth NR. Influence of polymers/excipients on development of agglomerated crystals of secnidazole by crystallo-co-agglomeration technique to improve processability. *Drug Development and Industrial Pharmacy*, **39(3)**, 437-46 (2013)

[46] Kawashima Y, Imai M, Takeuchi H, Yamamoto H, Kamiya K, Hino T. Improved flowability and compactibility of spherically agglomerated crystals of ascorbic acid for direct tableting designed by spherical crystallization process. *Powder Technology*, **130(1-3)**, 283-9 (2003)

[47] Cabiscol R, Finke JH, Zetzener H, Kwade A. Characterization of mechanical property distributions on tablet surfaces. *Pharmaceutics*, **10(4)**, 184 (2018)

[48] Kedia K, Wairkar S. Improved micromeritics, packing properties and compressibility of high dose drug, Cycloserine, by spherical crystallization. *Powder Technology*, **344**, 665-72 (2019)

[49] Jelić D, Papović S, Vraneš M, Gadžurić S, Berto S, Alladio E, et al. Thermo-analytical and compatibility study with mechanistic explanation of degradation kinetics of ambroxol hydrochloride tablets under non-isothermal conditions. *Pharmaceutics*, **13(11)**, 1910 (2021)

[50] French AD, Santiago Cintrón M. Cellulose polymorphy, crystallite size, and the Segal Crystallinity Index. *Cellulose*, **20**, 583-8 (2013)

[51] Skotnicki M, Jadach B, Skotnicka A, Milanowski B, Tajber L, Pyda M, et al. Physicochemical characterization of a co-amorphous atorvastatin-irbesartan system with a potential application in fixed-dose combination therapy. *Pharmaceutics*, **13(1)**, 118 (2021)

[52] Broza YY, Vishinkin R, Barash O, Nakhleh MK, Haick H. Synergy between nanomaterials and volatile organic compounds for non-invasive medical evaluation. *Chemical Society Reviews*, **47(13)**, 4781-859 (2018)

[53] Enyoh CE, Verla AW, Qingyue W, Ohiagu FO, Chowdhury AH, Enyoh EC, et al. An overview of emerging pollutants in air: Method of analysis and potential public health concern from human environmental exposure. *Trends in Environmental Analytical Chemistry*, **28**, e0010 (2020)